HHS Public Access

Author manuscript

*Int Conf Manip Autom Robot Small Scales*. Author manuscript; available in PMC 2024 July 03.

Published in final edited form as:

*Int Conf Manip Autom Robot Small Scales*. 2023 October ; 2023: . doi:10.1109/marss58567.2023.10294166.

# Closed Loop Control of Bubble-Propelled Microrobots

**Yanda Yang**[1], **David Rivas**[1], **Max Sokolich**[1], **Sambeeta Das**[1]

[1]Department of Mechanical Engineering, University of Delaware, Newark, DE 19716, United States

## Abstract

Bubble-propelled microrobots have an advantage of relatively swift movement compared to most other types of microrobots, which makes them well suited for applications such as micromanipulation or movement in flows, but their high speed also poses challenges in precisely controlling their motion. This study proposes automated control of the microrobots using visual feedback and steering with uniform magnetic fields to constrain the microrobot's moving direction. The implementation of a closed-loop control mechanism ensures precise autonomous navigation along prescribed trajectories. Experimental results demonstrate that this approach achieves satisfactory tracking performance, with an average error of 6. 7 $\mu$m for a microrobot with a diameter of 24 $\mu$m.

### Keywords

Microrobots; Active Matter; Closed loop control; Patchy Particles

## I. INTRODUCTION

Robots play a vital role in modern society, with many aspects of human production and daily life utilizing robotics. Similarly, in the microscale world, microrobots can be used for tasks like cell manipulation and drug delivery, providing crucial support for the development of biology and medicine. However, controlling these microrobots presents a significant challenge. Unlike conventional robots, microrobots are too small (specifically, on the micrometer scale) to accommodate various electronics like CPUs, sensors, and batteries. Nevertheless, we can drive them using some special mechanisms, such as magnetic fields, light, acoustic waves, and chemical actuation[1], [2], [3], [4], [5], [6].

One of the potential significant advantages of using microrobots, micron scale objects capable of carrying out desired tasks, for biomedical, micromanipulation, or other applications, is the precision that they can provide over more conventional techniques that rely on larger, tethered, devices [7], [8], [9], [10]. This precision is due to their small size, and also their untethered nature which allows for control in hard to reach and enclosed areas, such as in small vessels or inside microfluidic chips [11], [12], [13]. To take full advantage of this potential, however, precise control strategies are needed. Removing the

robotyyd@udel.edu .

human controller in favor of automated mechanism not only provides for potentially more precise control of the microrobot trajectory, but also one can imagine programming the microrobot to perform a wide range of automated tasks, eliminating otherwise monotonous tasks and increasing efficiency. Recently, we used patchy bubble-propelled microrobots for micromanipulation of passive objects into various shapes, thus demonstrating their potential use in micromanipulation and microfabrication applications [14]. These bubble-propelled spherical microrobots were coated in a patch of platinum which acts as a catalyst to the hydrogen peroxide in their liquid medium. They create oxygen by the catalytic decomposition of the peroxide which also produces bubbles that grow and burst at a consistent rate. The production of oxygen and the bubble growth and burst results in their dynamics and propulsion.

Bubble-propelled microrobots of various shapes and designs have been studied previously [15], [16], [17], [18]. One feature that makes these microrobots particularly intriguing for manipulation is their large speed and power compared to nearly every other type of microrobot [19], [20]. Their fast speed also can make precise positioning difficult however, therefore developing a means of automated control would be highly beneficial.

One means to obtain additional control is to use a computerized closed-loop strategy [21]. This has been employed previously to more precisely control microrobots [22], [23], [24], [25], [26], [27]. A closed-loop system works by continuously adjusting the control parameters based on the current feedback of the microrobot motion in order to guide it to a specified location or follow a predefined path. We have previously employed a closed-loop algorithm for the control of catalytic microrobots [12], and here we use our closed-loop control system to steer the much faster bubble-propelled microrobots along desired trajectories. We show that the microrobots can be made to follow the trajectories with fairly high precision, despite their fast speeds. This work therefore could be relevant in future micromanipulation or microfabrication applications.

In this study, we employ silica-based microrobots coated with platinum and nickel to implement a closed-loop control mechanism, ensuring precise autonomous navigation along the prescribed trajectory as illustrated in Fig. 1. We distinctively define discrete and continuous trajectories, subsequently evaluating the algorithm’s performance. The experiment results suggest that the bubble-propelled microrobot demonstrates impressive tracking capabilities, maintaining an average error below 10 $\mu$m.

## II. MATERIALS AND METHODS

### A. Fabrication of Microrobots

The microrobots were made according to the methods outlined in [14]. Briefly, 24 $\mu$m diameter paramagnetic polystyrene spheres were half-coated with a 20 nm layer of platinum using e-beam deposition, as shown in Fig. 2. The microrobots were suspended in a tube with DI water and around 1 $\mu$L of the suspension was added to 140 $\mu$L of 30% wh̆ydrogen peroxide and allowed to incubate for 30–40 minutes. This purpose is to make the Pt-catalyzed $H_2O_2$ chemical reaction more stable. The microrobots and hydrogen peroxide solution were then pipetted onto a square glass slide which was plasma cleaned for

approximately 1 hour to improve the hydrophilicity of the surface of the slide. This allows for complete spreading of the droplet on the surface of the slide, and hence produce a very flat surface, which avoid the microrobots being concentrated in the middle to generate too many bubbles. In addition, the plasma cleaner can also remove surface contamination of the slides and reduce possible interference to the experiment. Once on the slide, the microrobots produce oxygen bubbles which cause them to rise to the liquid-air interface where they self-propel. We allow the mixture to sit on the slide for 10 minutes before working on the control system. This purpose is to eliminate the drift of the microrobots with the water flow at the beginning and enhance the stability of the system work.

The microrobots were steered using magnetic fields produced by a 3D Helmholtz coil system.

## B. Experiment Setup

The Helmholtz coil system is fixed on a Zeiss Axiovert 200 M inverted microscope as depicted in Fig. 3. We designed the coil system and stage using SolidWorks, with PLA+ as the material for 3D printing. Our system integrates three pairs of orthogonal Helmholtz coils, each with differing dimensions, wrapped with 24 A WG copper wire. The smaller and medium-sized coils contain approximately 360 turns, while the largest coil comprises around 260 turns. The hardware of our closed-loop control system is illustrated in Fig. 4. The coils are operated by a separate Arduino control module, which is comprised of an Arduino Mega 2560, multiple H-Bridge Drivers, and a power supply unit. The Arduino module receives signals via the USB port from the PC. A FLIR BFS-U3–50S5C-C camera, connected to the PC through USB, is used to visualize the microscopic scale.

## C. Control Algorithm

To control the microrobot's moving direction, we primarily need to control its orientation within the plane. Since bubbles are generated continuously from the Pt surface, the resulting thrust persistently acts on the microrobot. Thus, without a magnetic field, the microrobot's movement would be random. However, upon activating the magnetic field, a two-dimensional (2D) coordinate system, with the spherical center of the microrobot as the reference point in the plane, is established as illustrated in Fig. 5. The components of the 2D joint magnetic field, represented by $\boldsymbol{B_x}$ and $\boldsymbol{B_y}$, are generated by two corresponding pairs of Helmholtz coils. To orient the microrobot, we must create a uniform magnetic field which applies a torque to the positioned microrobot - equal to the cross product of the magnetic moment and the magnetic field:

$$\boldsymbol{\tau} = \boldsymbol{\mu} \times \boldsymbol{B}. \tag{1}$$

**Algorithm 1:** 2D Closed Loop Control of Orienting

**Data:** initial magnetic field $B_0$, distance threshold $\Theta$, desired tracjectory $T$.
**Result:** actual trajectory $T^{'}$.
*initialize magnetic field* $B$ *as* $B_0$;
**while** $n \leq N$ **do**
  *get current position* $(x_r, y_r)$ *and store it in* $T^{'}$;
  *get target point* $(x_n, y_n)$;
  *calculate absolute distance*
  $d \leftarrow \sqrt{(x_n - x_r)^2 + (y_n - y_r)^2}$;
  **if** $d > \Theta$ **then**
    *apply magnetic field* $B$;
    *get new position* $(x_r^{'}, y_r^{'})$;
    *calculate target angle* $\alpha_t \leftarrow \tan^{-1}\left(\frac{y_n - y_r^{'}}{x_n - x_r^{'}}\right)$;
    *calculate actual angle* $\alpha_t \leftarrow \tan^{-1}\left(\frac{y_r^{'} - y_r}{x_r^{'} - x_r}\right)$;
    *get error* $e$ *as the difference between* $\alpha_t$ $\alpha_a$;
    *update* $B \leftarrow \begin{bmatrix} \cos e & -\sin e \\ \sin e & \cos e \end{bmatrix} \cdot B$;
  **end**
  **if** $d \leq \Theta$ **then**
    *update* $n \leftarrow n + 1$;
  **end**
**end**
*return* $T^{'}$;

The Algorithm 1 illustrate the closed loop control of the bubble-propelled microrobot. The initial magnetic field produced by two pairs of the Helmholtz coils can be represented as:

$$\boldsymbol{B} = \begin{bmatrix} \boldsymbol{B}_x \\ \boldsymbol{B}_y \end{bmatrix} = \begin{bmatrix} \boldsymbol{B}_0 \\ \boldsymbol{B}_0 \end{bmatrix}. \tag{2}$$

To implement closed-loop control, we first need to define a trajectory. This is achieved by using the mouse to sketch a random line or shape on the screen displaying the real-time camera view. The trajectory can be considered as comprising $N$ points. With the aid of the OpenCV library, the coordinates of these points are extracted and stored in an array as follows:

$$T = [(x_1, y_1), (x_2, y_2), \ldots, (x_N, y_N)]. \tag{3}$$

Additionally, the OpenCV library aids in identifying the contour of the microrobot, thereby providing the microrobot's coordinates. Subsequently, the absolute distance $d$ between the current position of the microrobot $(x_r, y_r)$ and the target point $(x_n, y_n)$ is computed. If $d$ is less than or equal to a threshold $\Theta$, the target point is switched to $(x_{n+1}, y_{n+1})$. Conversely, if $d$ exceeds the threshold, the error between the target direction and the actual direction of the microrobot is calculated. This error, $e$, denotes the angle at which the field should be rotated in order to guide the microrobot towards the target point. As previously mentioned, we can generate a torque on the microrobot by adjusting the magnetic field direction, allowing

the microrobot to orient. By utilizing the rotation matrix in two-dimensional space, the new magnetic field can be continuously updated through left multiplication by the rotation matrix:

$$\boldsymbol{R} = \begin{bmatrix} \cos e & -\sin e \\ \sin e & \cos e \end{bmatrix} \tag{4}$$

We have previously employed this control method to guide catalytic microrobotsto direct them towards a desired target or along a specified path [12]. Although proportional integral derivative (PID) algorithms are commonly employed in closed-loop control methods, they require tuning of the coefficients of each term which can be cumbersome and change depending on the specific experimental conditions. Additionally, a PID algorithm requires time to adapt to a sudden change in the desired output, therefore it may not handle abrupt turns easily. However, our algorithm maintains a single parameter, the angle between the applied magnetic field and the direction of microrobot motion, and therefore does not require time to adapt for a sharp turn.

## III. RESULTS AND DISCUSSION

### A. Open Loop Control

In our setup, we can steer the microrobots using open-loop control via a wireless controller. The joystick of this controller, capable of full 360° rotation, allows for comprehensive directional control. Manipulating the joystick in a specific direction sends a corresponding signal to the control module, which subsequently modulates the current supplied to the coil. This in tum changes the direction of the uniform magnetic field, enabling the microrobot to orient to the desired direction. Additionally, the magnitude of the magnetic field can be altered by varying the degree to which the joystick is pushed. As per Equation 1, this generates increased torque—a useful feature in instances where bubble-propelled microrobots are required to execute sharp turns. Fig. 7(A) and supporting video illustrate the movement of bubble-propelled microrobots when a magnetic field is applied for orientation. Based on our computational simulations, the bubble-propelled microrobot can achieve a locomotion speed of approximately 300 $\mu$m/s, as shown in Fig. 6.

### B. Closed Loop Control

In order to realize trajectory tracking, a closed-loop control system was implemented with the primary aim of directing the microrobots along a specified path, from the start to the endpoint. Within this system, a specific microrobot is selected to be tracked along the desired trajectory. The user outlines this trajectory on the computer screen, utilizing the image captured by the camera.

The performance of the closed-loop control system was evaluated via three defined trajectories: discrete, continuous, and a combination of continuous-discrete, as evidenced in Fig. 7(B). These trajectories were manually drawn by the user. Discrete trajectories are delineated by discrete nodes. These nodes are connected with straight lines, forming

several straight line segments. Such discrete trajectories primarily test the linear movement capability of the microrobot and its ability to make sharp turns. When following a straight line, the microrobot's target point remains consistently at the endpoint of the line segment. As such, the algorithm continually readjusts the microrobot's movement direction to approximate the target point.

Continuous trajectories are determined by continuous nodes, and a multitude of minuscule straight line segments collectively form a smooth curve. As the microrobot follows the curve, it persistently updates its next target point. Experimental results indicate superior performance of the microrobot when tracking the continuous trajectory. Except for minor vibrations and disturbances, the microrobot barely deviates from the prescribed trajectory.

We also experimented with defining a continuous trajectory initially, followed by a discrete trajectory. This was done to compare the tracking performance of the two trajectory types under identical conditions. Observations revealed that the microrobot performed excellently and barely deviated from the trajectory in the part of the continuous curve trajectory. However, when it went to the part of the discrete straight-line trajectory, the microrobot deviated sometimes again. We observed the difference in the trajectory tracking performance of bubble-propelled microrobots between discrete and continuous trajectories, and we thought several factors may contribute to this phenomenon. Discrete trajectories, defined by relatively distant nodes connected by straight lines, inherently need more precise control due to the need for the microrobot to maintain a strict linear path. However, continuous trajectories, defined by continuous nodes forming a smooth curve, offer greater tolerance for minute adjustments, which could facilitate more accurate tracking. In addition, the abrupt directional changes in discrete trajectories might cause larger errors, while the smooth, incremental directional adjustments in continuous trajectories could lead to a better performance.

In this study, we performed an evaluation of the trajectory errors between the actual and prescribed positions. For each corresponding pair of actual and prescribed points, we calculated the Euclidean distance to represent the positional error at that instance. Subsequently, we calculated the average error over all instances by summing all the Euclidean distances and dividing by the total number of instances. Finally, the distribution of these errors was visualized using a box plot, with the calculated average error represented by a red dot on the plot.

Based on our evaluation, the microrobot followed the prescribed path with an average error of less than 10 $\mu$m in continuous instance and around 50 $\mu$m in discrete instance, as shown in the box plot of Fig. 7(B). Supporting videos display the real footage of the microrobot successfully navigating the trajectory. The microrobot completed the entire path within 30 seconds, propelled solely by the bubbles generated. These outcomes hold significant promise for the field of self-propelled rnicrorobot control, as they demonstrate the feasibility of navigating a microrobot along a prescribed trajectory for diverse applications.

## IV. CONCLUSIONS AND FUTURE WORK

In this study, we have successfully demonstrated the closed-loop control of the bubble-propelled rnicrorobots. We used the propulsion capabilities of the bubbles generated by the rnicrorobot and magnetic fields produced by Helmholtz coils to manage its steering. The findings of this research highlight our ability to control this fast-moving, bubble-propelled microrobot with high precision. The average error of the microrobots following the continuous trajectory is only 6.7 $\mu$m for a 24 $\mu$m rnicrorobot, as shown in the continuous trajectory box plot in Fig. 7(B). This ability opens up opportunities for precise navigation and targeted delivery, providing considerable potential for future micromanipulation or microfabrication applications.

Looking forward, there are several interesting possibilities for future research. These include improving the control algorithm to enhance the bubble-propelled microrobot's performance in discrete trajectories — specifically, its ability to move in a straight line, expanding the closed-loop control from a two-dimensional plane to three dimensions, and integrating a z-field to the closed loop algorithm which is capable of accelerating the microrobot [28]. Also implementing an automated micromanipulation algorithm could be beneficial in future applications involving precise micromanipulation or micro fabrication.

The microrobot control methodology shown in this work offers significant potential for researchers and scientists engaged in the micro and nano domains. It offers numerous opportunities for high-precision tasks and progress in various fields.

## ACKNOWLEDGEMENTS

This work was supported by the National Science Foundation under grant GCR 2219101 and the National Health Institute under grant 1R35GM147451. This project was also supported with a grant from the National Institute of General Medical Sciences – NlGMS (5P20GM109021-07) from the National Institutes of Health and the State of Delaware.

## References

[1]. Das S, Steager EB, Stebe KJ, and Kumar V, "Simultaneous control of spherical microrobots using catalytic and magnetic actuation," in 2017 International Conference on Manipulation, Automation and Robotics at Small Scales (MARSS). IEEE, 2017, pp. 1–6.

[2]. Das S, Hunter EE, DeLateur NA, Steager EB, Weiss R, and Kumar V, "Controlled delivery of signaling molecules using magnetic microrobots," in 2018 international conference on manipulation, automation and robotics at small scales (MARSS). IEEE, 2018, pp. 1–5.

[3]. Beaver LE, Wu B, Das S, and Malikopoulos AA, "A first-order approach to model simultaneous control of multiple microrobots," in 2022 International Conference on Manipulation, Automation and Robotics at Small Scales (MARSS). IEEE, 2022, pp. 1–7.

[4]. Rivas D, Mallick S, Solrolich M, and Das S, "Cellular manipulation using rolling microrobots," in 2022 International Conference on Manipulation, Automation and Robotics at Small Scales (MARSS). IEEE, 2022, pp. 1–6.

[5]. Rivas DP, Sokolich M, and Das s., "Spatial patterning of micromotor aggregation and flux," ChemNanoMat, p. e20230022S.

[6]. Shah ZH, Wu B, and Das S, "Multistimuli-responsive microrobots: A comprehensive review," Frontiers in Robotics and AI, vol. 9, p. 1027415, 2022.

[7]. Ahmad B, Gauthier M, Laurent GJ, and Bolopion A, "Mobile microrobots for in vitro biomedical applications: A survey," IEEE Transactions on Robotics, vol. 38, no. 1, pp. 646–663, 2022.

[8]. Das S, Hunter EE, DeLateur NA, Steager EB, Weiss R, and Kumar V, “Cellular expression through morphogen delivery by light activated magnetic microrobots,” Journal of Micro-Bio Robotics, vol. 15, pp. 79–90, 2019.

[9]. Shah ZH, Sockolich M, Rivas D, and Das S, “Fabrication and open-loop control of three-lobed nonspherical janus microrobots,” MRS Advances, pp. 1–5, 2023. [PubMed: 37362909]

[10]. Sokolich M, Rivas D, Yang Y, Doey M, and Das S, “Modmag: A modular magnetic micro-robotic manipulation device,” MethodsX, vol. 10, p. 102171, 2023.

[11]. Mallick S, Abouomar R, Rivas D, Solrolich M, Kirmizitas FC, Dutta A, and Das S, “Doxorubicin-loaded microrobots for targeted drug delivery and anticancer therapy.” Advanced Healthcare Materials, pp. e2300939–e2300939, 2023. [PubMed: 37378647]

[12]. Solrolich M, Rivas D, Shah ZH, and Das S, “Automated control of catalytic janus micromotors,” MRS Advances, pp. 1–5, 2023. [PubMed: 37362909]

[13]. Rahman MM, Garudadri T, and Das S, “Role of surface tension in microrobot penetration in membranes,” in 2022 International Conference on Manipulation, Automation and Robotics at Small Scales (MARSS). IEEE, 2022, pp. 1–6.

[14]. Rivas DP, Sokolich M, Muller H, and Das S, “Dynamics and control of bubble-propelled microrobots,” arXiv preprint arXw:2203.13257, 2022.

[15]. Villa K, Viktorova J, Plutnar J, Ruml T, Hoang L, and Pumera M, “Chemical microrobots as self-propelled microbrushes against dental biofilm,” CeU Reports Physical Science, vol. 1, no. 9, p. 100181, 2020. [Online]. Available: https://www.scieocedirectcom/science/article/pii/S2666386420301922

[16]. Solovev AA, Sanchez S, Pumera M, Mei YF, and Schmidt OG, “Magnetic control of tubular catalytic microbots for the transport, assembly, and delivery of micro-objects,” Advanced Functional Materials, vol. 20, no. 15, pp. 2430–2435, 2010. [Online]. Available: https://onlinelibrary.wiley.com/doilahs/10.1002/adfm.200902376

[17]. Manjare M, Yang B, and Zhao Y-P, “Bubble driven quasioscillatory translational motion of catalytic microm.otors,” Phys. Rev. Lett, vol. 109, p. 128305, Sep 2012. [Online]. Available: https://link.aps.org/doi/10.1103/PhysRevLett.l09.128305 [PubMed: 23005998]

[18]. Wrede P, Medina-Sánchez M, Fomin VM, and Schmidt OG, “Switching propulsion mechanisms of tubular catalytic micromotors”: Small, vol. 17, no. 12, p. 2006449, 2021. [Online]. Available: https://onlinelibrary.wiley.com/doi/ahs/10.1002/smll.202006449

[19]. Gao W, Sattayasamitsathit S, and Wang J, “Catalytically propelled micro-/nanomotors: how fast can they move?” The Chemical Record, vol. 12, no. 1, pp. 224–231, 2012. [Online]. Available: https://onlinelibrary.wiley.com/doilahs/10.1002/tcr.201100031 [PubMed: 22162283]

[20]. Zhang J, Zheng X, Cui H, and Silber-Li Z, “The self-propulsion of the spherical pt-sio2 janus micromotor;” Micromachines, vol. 8, no. 4, 2017. [Online]. Available: https://www.mdpi.com/2072-666X/8/4/123

[21]. Jiang J, Yang Z, Ferreira A, and Zhang L, “Control and autonomy of microrobots: Recent progress and perspective,” Advanced Intelligent Systems, vol. 4, no. 5, p. 2100279, 2022. [Online]. Available: https://onlinelibrary.wiley.com/doi/ahs/10.1002/aisy.202100279

[22]. Jiang J, Yang L, and Zhang L, “Closed-loop control of a helmholtz coil system for accurate actuation of magnetic microrobot swarms,” IEEE Robotics and Automation Letters, vol. 6, no. 2, pp. 827–834, 2021.

[23]. Rahman MA, Takahashi N, Siliga KF, Ng NK, Wang Z, and Ohta AT, “Vision-assisted micromanipulation using closed-loop actuation of multiple microrobots,” Robotics and Biomimetics, vol. 4, no. 1, p. 7, 2017. [Online]. Available: 10.1186/s40638-017-0064-4 [PubMed: 29152448]

[24]. Khalil ISM, Ferreira P, Eleuotério R, de Korte CL, and Misra S, “Magnetic-based closed-loop control of paramagnetic microparticles using ultrasound feedback,” in 2014 IEEE International Conference on Robotics and Automation (ICRA), 2014, pp. 3807–3812.

[25]. Barbot A, Decanini D, and Hwang G, “Local flow sensing on helical microrobots for semi-automatic motion adaptation,” The International Journal of RDbotics Research, vol. 39, no. 4, pp. 476–489, 2020. [Online]. Available: 10.1117/0278364919894374

[26]. Hao Z, Xu T, Huang C, Lai Z, and Wu X, “Modeliog and closed-loop control of ferromagnetic nanoparti.cles microrobots,” in 2020 IEEE International Conference on E-health Networking, Application & Services (HEALTHCOM), 2021, pp. 1–6

[27]. Yang L, Wang Q, and Zhang L, “Model-free trajectory tracking control of two-particle magnetic microrobot,” IEEE Transactions on Nanotechnology, vol. 17, no. 4, pp. 697–700, 2018.

[28]. Wang L, Chen L, Zheog X, Yu Z, Lv W, Sheng M, Wang L, Nie P, Li H, Guan D, and Cui H, “Multimodal bubble microrobot near an air–water interface,” Small, vol. 18, no. 39, p. 2203872, 2022. [Online]. Available: https://onlinelibrary.wiley.com/doilahs/10.1002/smll.202203872

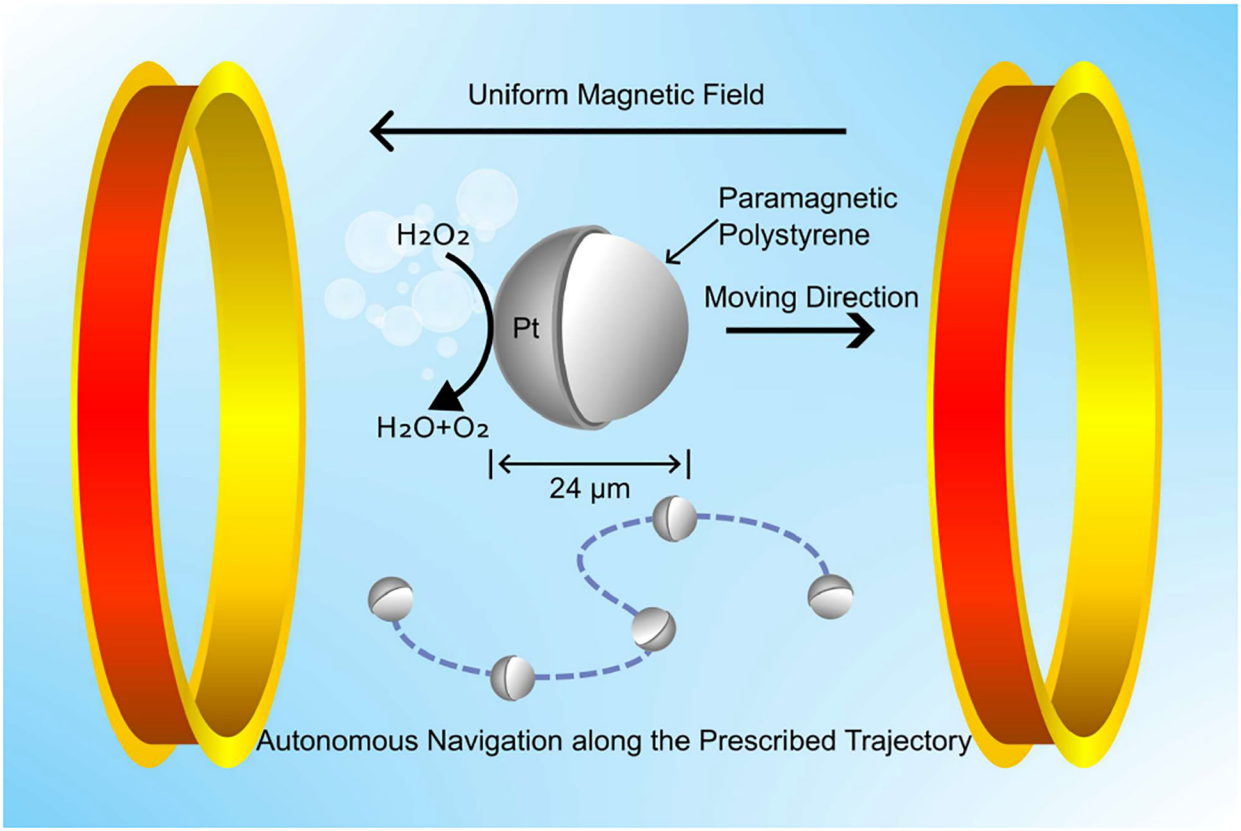


**Fig. 1:**
Schematic diagram of bubble-propelled microrobots working principle

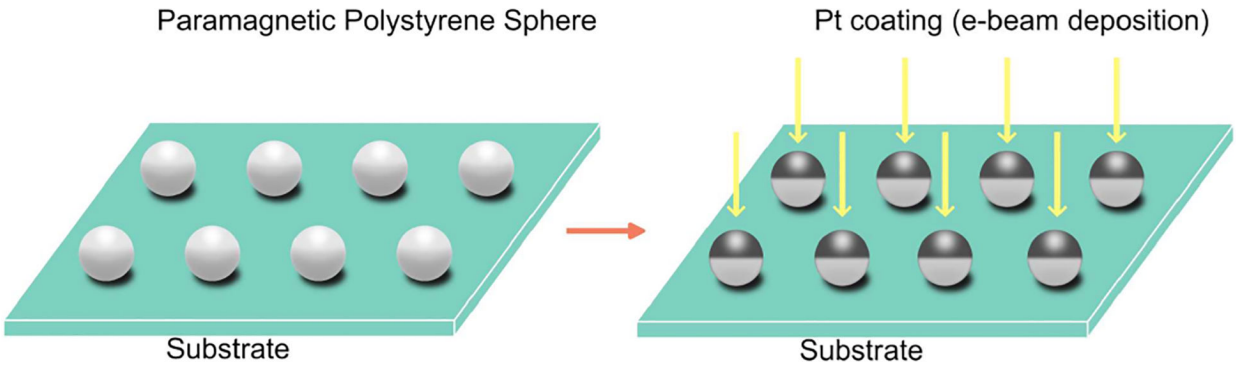


**Fig. 2:**
Fabrication of microrobots

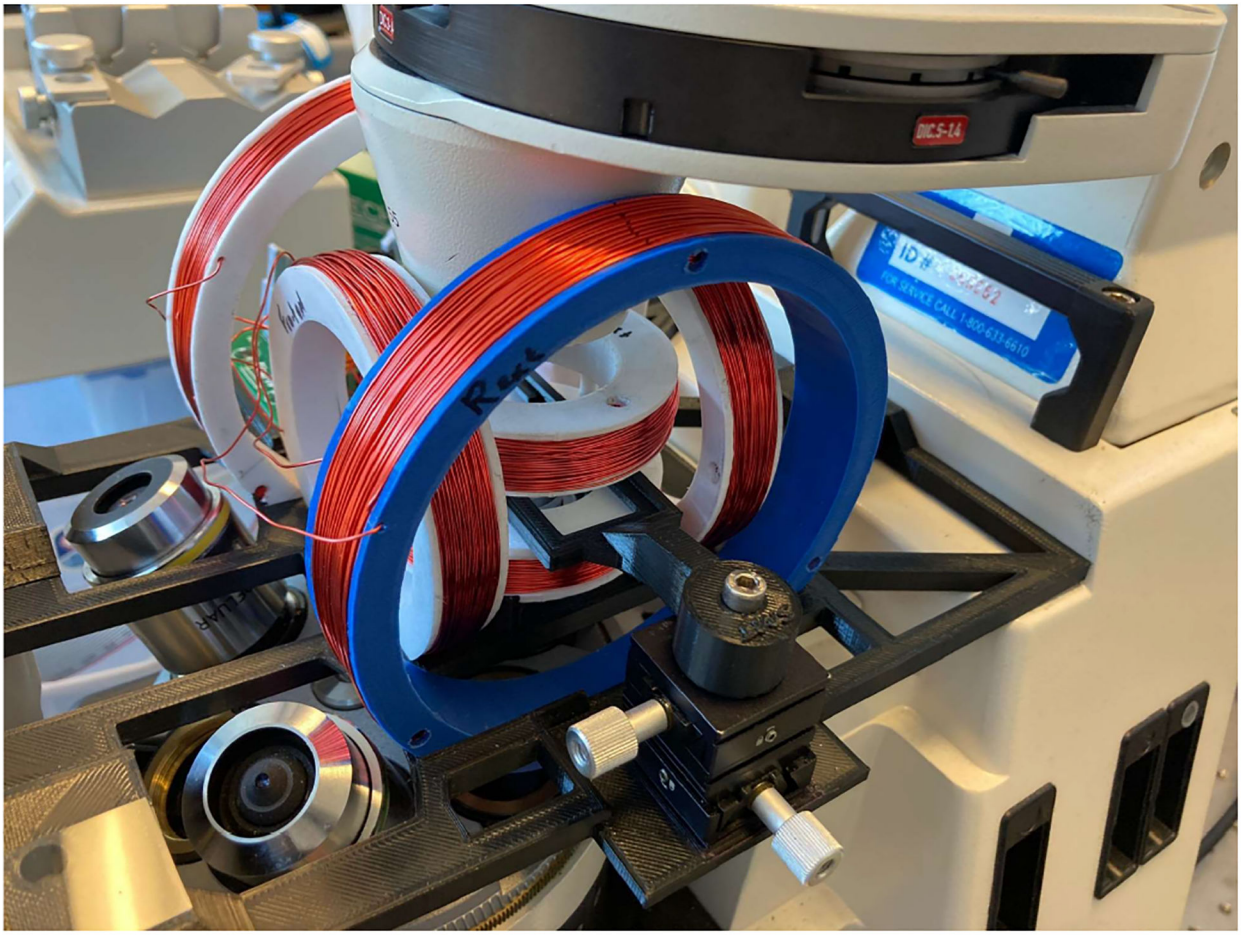

**Fig. 3:**
Helmholtz coils and experiment setup

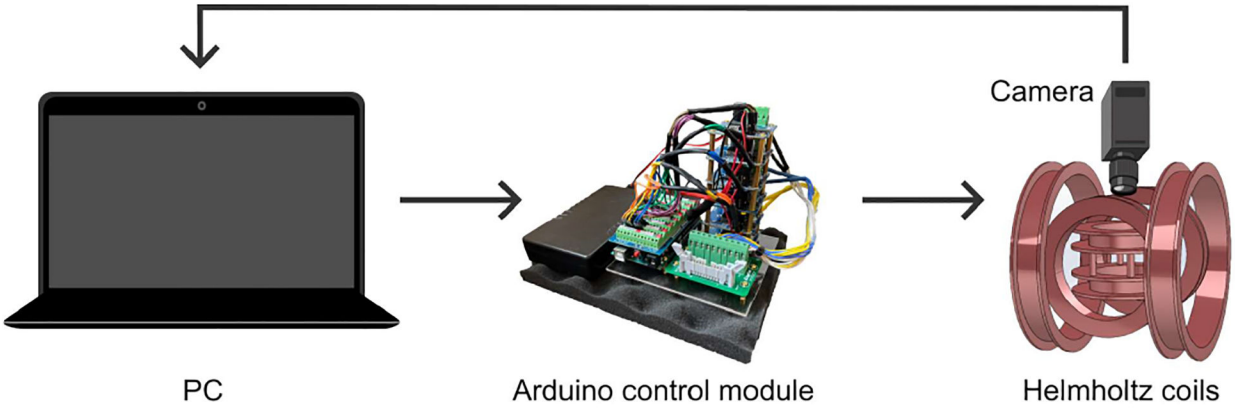


**Fig. 4:**
General overview of the closed loop control system

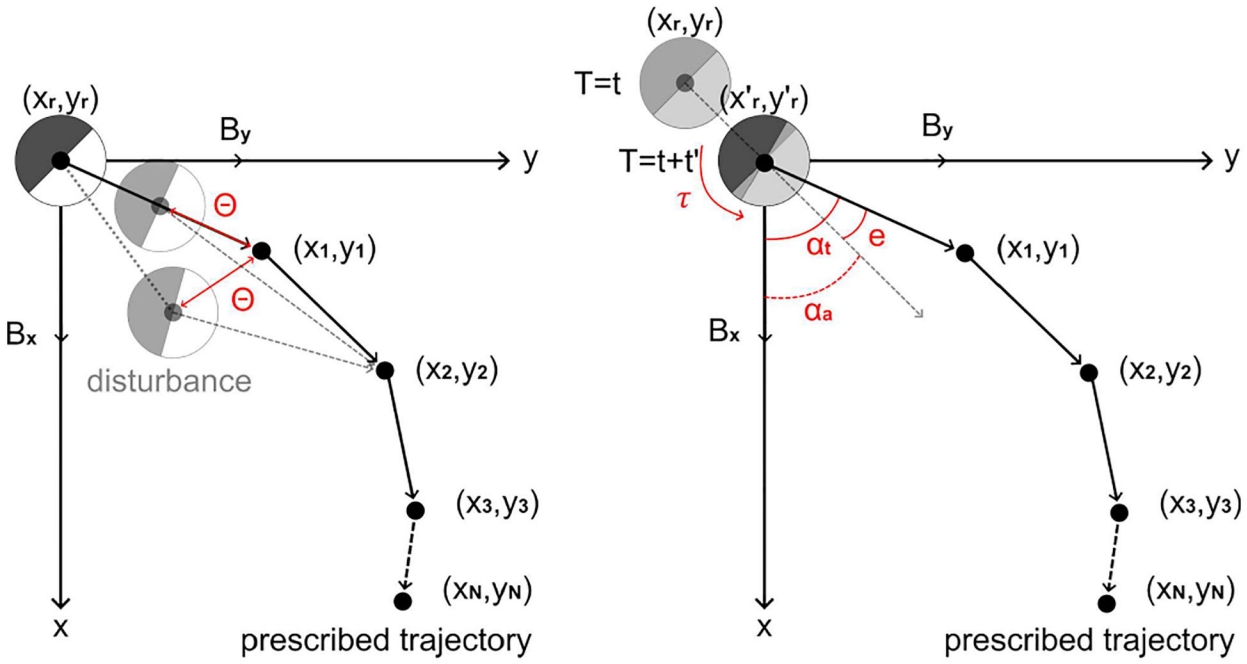


**Fig. 5:**
2D coordinate system model for the microrobot

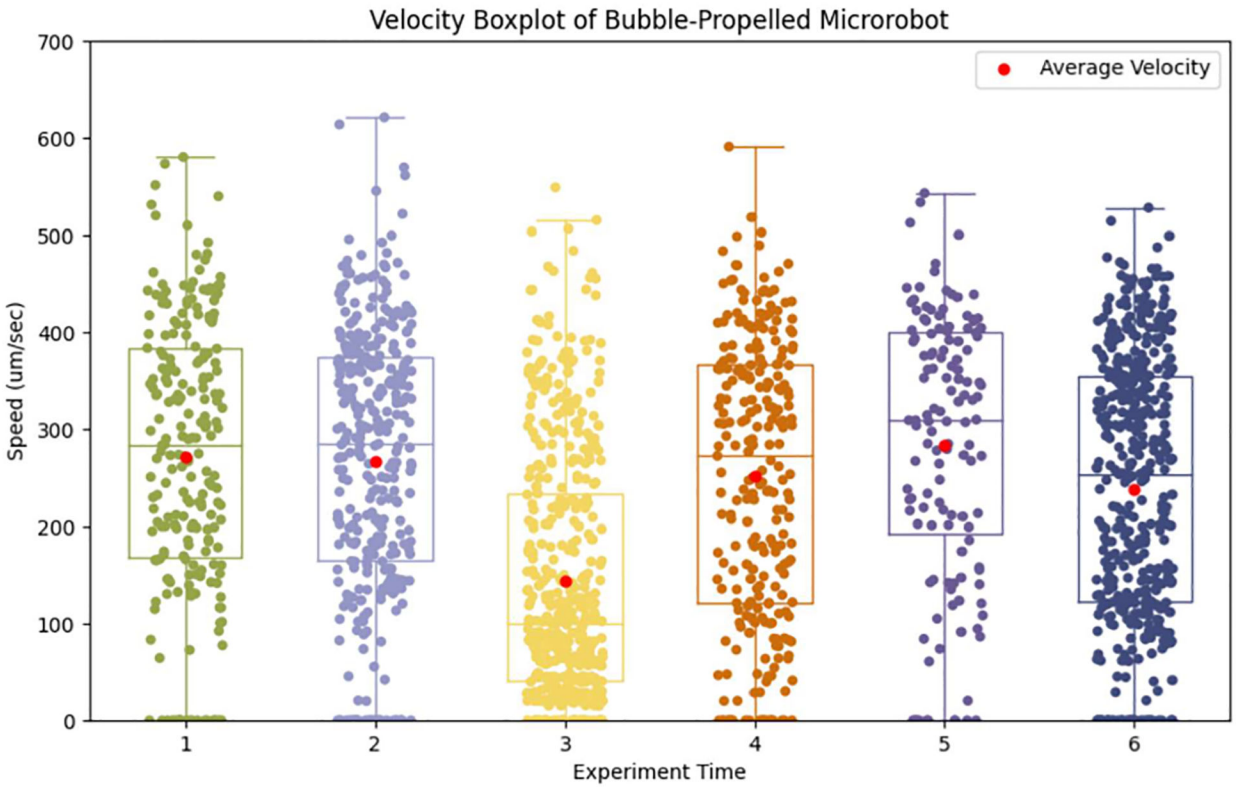


**Fig. 6:**
Velocity box plot of the microrobot open loop control experiments

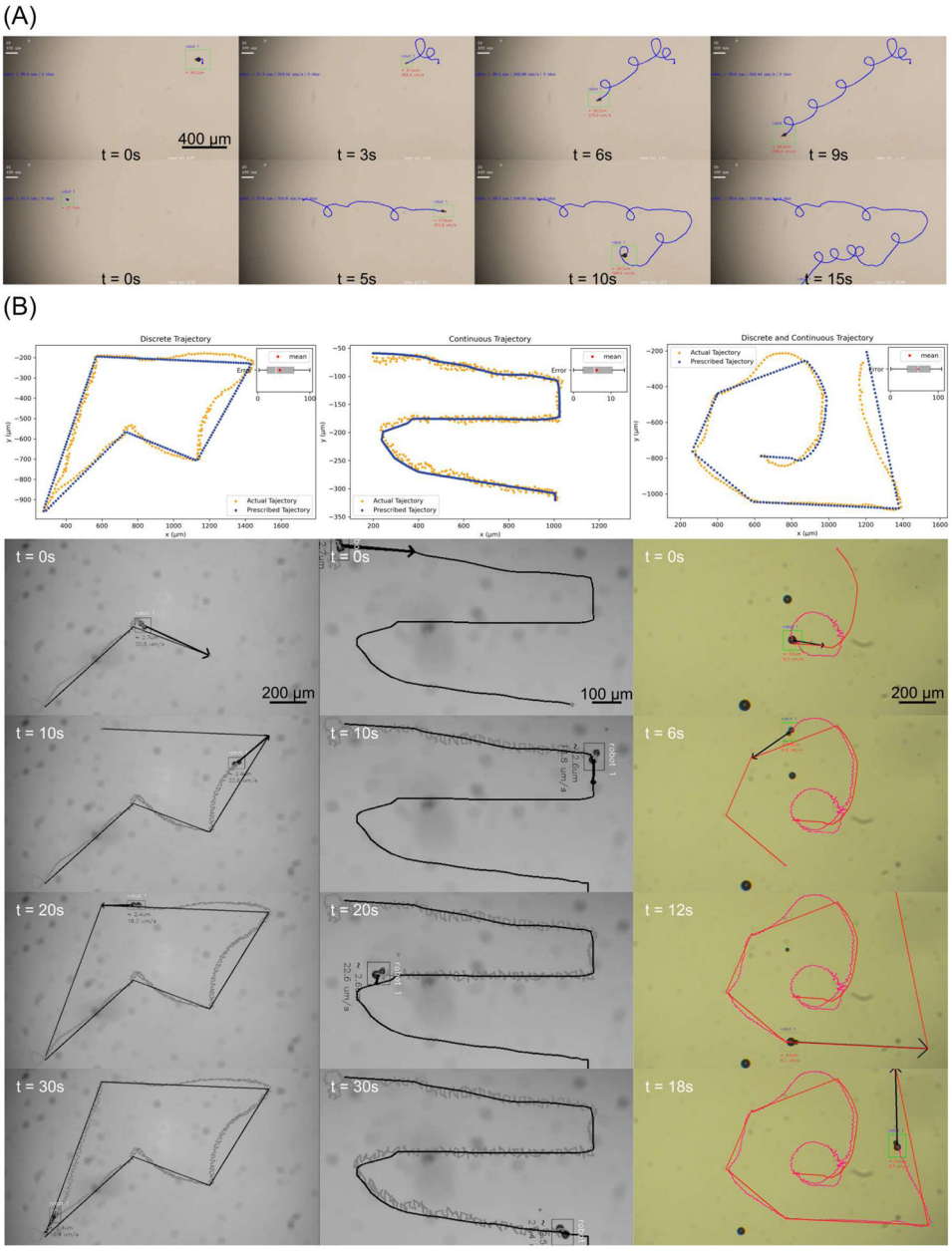


**Fig. 7:**

A. Bubble-propelled microrobot open loop control. B. Bubble-propelled microrobot following discrete, continuous, and their combined trajectories. The blue dots represent the desired trajectory and the orange dots represent the actual trajectory.